JOURNAL OF MATERIALS SCIENCE 27 (1992) 930–936

Effect of dynamic loading on tensile strength and failure mechanisms in a SiC fibre reinforced ceramic matrix composite

J. LANKFORD, H. COUQUE, A. NICHOLLS
Department of Materials Sciences, Southwest Research Institute, 6220 Culebra Road, San Antonio, Texas 78228-0510, USA

The tensile strength and associated failure micromechanisms have been characterized for a SiC fibrereinforced ceramic matrix composite subject to strain rates approaching 1000 s^{-1}. It is found that behaviour under such conditions is not described by the current matrix fracture/fibre pull-out models. This is a consequence of the rapid and extreme frictional heating produced at the fibre–matrix interface by sliding velocities on the order of 100 $m\,s^{-1}$. At sufficiently rapid loading rates, the near-interface matrix appears to melt, and the frictional interface shear resistance is reduced to the point that the fibres debond throughout the specimen, and pull out without failing. This suggests that for sufficiently rapid loading, the stress to fail the composite will approach that merely to create the initial matrix crack, i.e., a stress level well below the ultimate strength normally attainable under *quasi*-static conditions.

1. Introduction

Ceramic matrix composites reinforced with silicon carbide fibres are currently candidates for a variety of applications in which their nominal material and mechanical properties appear to be extremely desirable. However, an important performance consideration, i.e. their response to dynamic, or impulsive, tensile loading has not yet been explored, either theoretically or experimentally. This factor will surely be highly relevant to a number of potential applications, and deserves careful study.

This is not to say that the effect of loading rate, *per se*, on fibre–matrix interaction has not received study; in fact, it has. Goettler and Faber [1], for example, have shown that the interfacial shear strength within the SiC fibre-borosilicate glass system increases with stress rate. On the other hand, Phillips [2] has observed that both the work of fracture and fibre pull-out length are constant with increasing rate of loading for carbon fibre reinforced lithium aluminosilicats (LAS) pyroceram. However, it should be noted that the fibre sliding rates in these experiments were low, on the order of 10^{-7}–10^{-4} $m\,s^{-1}$. Under impulsive loading conditions, fibre sliding rates may attain velocities well in excess of 100 $m\,s^{-1}$.

The mechanisms responsible for the excellent and unusual (for a ceramic) *quasi*-static strength, deformation, and toughness of fibre reinforced ceramics have been thoroughly reviewed [3]. Basically, good fibre reinforced ceramics exhibit tensile stress–strain behaviour as shown in Fig. 1. The initial deviation from linearity, σ_O, corresponds to the formation of the first crack in the matrix, which extends entirely across the specimen, breaking very few fibres on route. With increased loading, other matrix cracks are initiated, whose spacing distribution is characteristic of the frictional stress transfer afforded by the fibre–matrix interface. Further non-linear deformation is produced by unbroken fibres sliding within these crack-created blocks of matrix material. Once the specimen gauge section is full of cross-sectional matrix cracks, the surviving fibre bundles begin to fail, i.e. the ultimate strength, σ_U, has been attained. Any further tail in the stress–strain curve is caused by broken fibre pull-out. This mechanism has been validated [3–6], but only for what amounts to *quasi*-static rates of loading.

The specific parameter that determines the rate of load transfer from the fibres to the matrix, and thus the ultimate strength of the composite, is simply the frictional resistance to fibre pull-out. For micromechanics purposes, it is convenient to treat the latter as an effective shear stress, τ, characteristic of a debonded interface. However, from a materials response viewpoint, it is more relevant [3] to view τ (to a first order) as μq_N, where μ is a classic friction coefficient, and q_N is the residual stress normal to the interface. Thus, the question at issue reduces to the effect of dynamic loading upon μ and q_N.

The study of sliding friction between ceramic couples indicates that μ generally increases with sliding velocity; such behaviour is primarily a consequence of the interfacial temperature rise associated with rapid sliding. Under steady state sliding conditions, the local temperature may rise hundreds of degrees [7], promoting local plasticity and thermal expansion. For the case of fibres sliding within a confined space, thermally-induced dimensional changes would tend to alter q_N, while the softening of

0022–2461

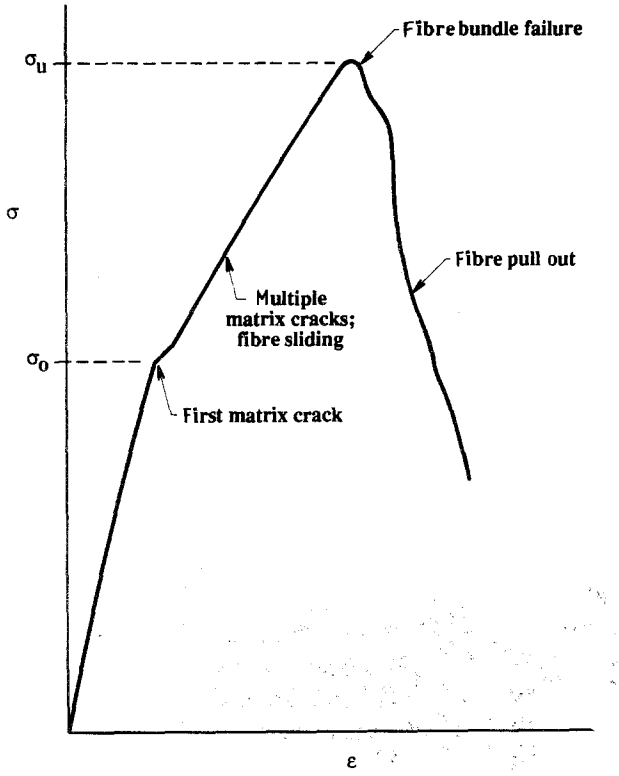

Figure 1 Fiber-reinforced composite stress-strain response and associated damage processes.

interface constituents, permitting frictional energy-absorbing plasticity, would be reflected in μ. In this regard, it is relevant to note that for LAS pyroceram couples sliding under ambient conditions, an increase in the sliding velocity from 0.5 to 1.8 m s^{-1} doubled the friction coefficient [7]. After 500 s of sliding at each velocity, corresponding near-interfacial temperatures were 110 and 450 °C, respectively. Moreover, measurements of fibre displacement caused by *quasi*-static microhardness indentation indicate [8] that for strong, tough SiC fibre reinforced pyroceram, the fibre/matrix friction coefficient may be as low as 0.01; under these circumstances, i.e. low sliding velocity, frictional temperature increases are negligible. However, in light of the apparent small amplitude of μ, combined with its major role in the composite failure process, it is clear that changes induced in it by dynamic loading could have a profound effect on both strength and (effective) ductility.

The objective of the present work is to explore the effect of high strain rates upon the tensile failure process in a representative fibre reinforced ceramic matrix composite. It will be seen that the results must be interpreted in terms of thermal effects at the fibre/matrix interface.

2. Material

The composite chosen for study was fabricated* by United Technologies (UTRC), and has been characterized microstructurally by Brennan [10]. Briefly, the panel from which the specimens were extracted was laid up unidirectionally using 46 v/o Nicalon silicon carbide fibres; the latter are approximately 16 μm in diameter. The matrix was the UTRC lithium-aluminosilicate glass ceramic designated as LAS-II, which is essentially Corning 9608 pyroceram modified by replacing 3 w/o TiO_2 with 3 w/o ZrO_2, and adding 5 w/o Nb_2O_5. After fabrication, the composite is ceramed, or crystallized, by heat treatment at 1050 °C for 2 h. The resulting matrix consists of grains ranging in size from $\sim$ 0.5–2.0 μm, crystallized in the β-quartz-silica solid solution LAS phase. However, the microstructure is different near the fibre–matrix interface: next to the fibre is an extremely thin layer of eta aluminum, contained within an adjacent matrix ring of very fine NbC precipitates. In addition, the fibres themselves are altered by the processing, their outer layer consisting of a 20–40 nm thick ring of almost pure carbon. This carbon-rich zone is weakly bonded to both the matrix and the fibre, and is thought [8] to be responsible for the low value of the *quasi*-static fibre–matrix sliding friction coefficient.

3. Experimental procedure

3.1. Mechanical testing

Test coupons with fibres parallel to the tensile axis were sectioned from plate material; in this form, the coupons consisted of simple cylinders 35 mm long and 3 mm diameter. The coupons were modified by using a shaped grinding wheel to generate a reduced mid-section characterized by an 8.9 mm gauge length and a 2.05 mm diameter. These specimens were then bonded into internally threaded steel sections, using high strength epoxy.

Quasi-static experiments were performed using a standard servo-hydraulic test machine under displacement control at a constant strain rate of 10^{-5} s^{-1}. However, to promote pure axial loading, load transfer was accomplished by means of thin, flexible, steel cables (Fig. 2) threaded into the specimen grips. Strain

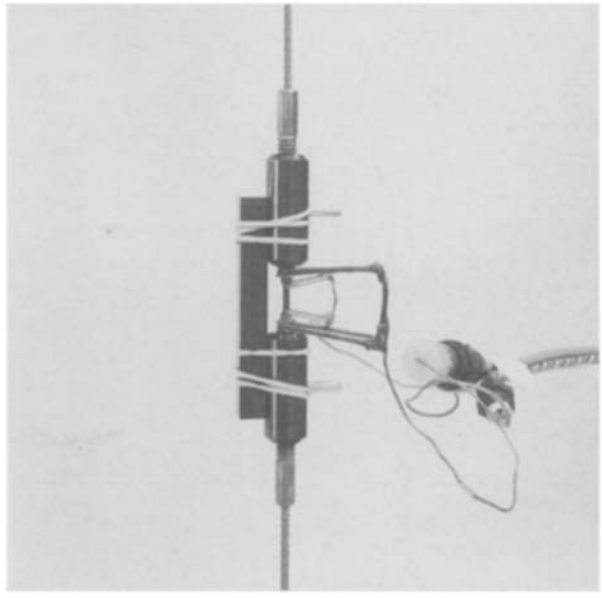

Figure 2 Quasi-static tensile test set-up.

* Panel 2391 [9]

was measured over the entire specimen using an extensometer.

Dynamic tensile tests utilized a split Hopkinson pressure bar (SHPB) modified for tensile testing [11]. The test set-up consists of a split collar placed about a button head tensile specimen as shown in Fig. 3. An incident compressive stress wave, generated from the impact of a projectile striker bar at one end of two long bars in series, is transmitted through the insert from one bar to the other, leaving the specimen intact. A tensile wave is then reflected from the free end of the SHPB, causing the specimen to be loaded in tension. Axially-symmetric play of each thread of the tensile specimen is ensured by means of a Teflon guide. From the strain record of the transmitted and reflected pulses in the pressure bars, the stress and the strain rate, respectively, are deduced [1], and by integrating the strain rate with respect to time, strain versus time is generated. The stress–strain curve is finally obtained by eliminating time. The strain record includes the deformation of both the specimen gauge section and the bonding film between the specimen and the steel insert. An estimate of the strain within the bonding film was obtained based on photographs of the specimen/insert junction before and after testing. The value found (< 0.002) indicates that the measured elastic strain (about 0.02) predominantly reflected the response of the specimen. On the other hand, transient dynamic effects make it difficult to interpret the initial portion of the strain gauge-derived specimen strain signal in terms of accurate elastic modulus or yield point values [11].

Since it will be seen that the present composites are ductile under certain conditions, it should be noted that when this happens, the dynamic strain rate is not constant. Initially, a constant stress rate ($\dot{\sigma}$) ramp is imposed, lasting for approximately 10–20 μs; during this regime, the strain rate $\dot{\varepsilon}$ is equal to $\dot{\sigma}/E$, where E is the elastic modulus of the composite. However, should the specimen yield, the strain rate will instantaneously increase due to the lower (effective) modulus, and will be reflected in the stress-time history recorded by the SHPB strain gauges. It should be noted that the elastic strain rate can be varied somewhat by controlling the velocity of the striker bar; in particular, the stress rate increases with velocity.

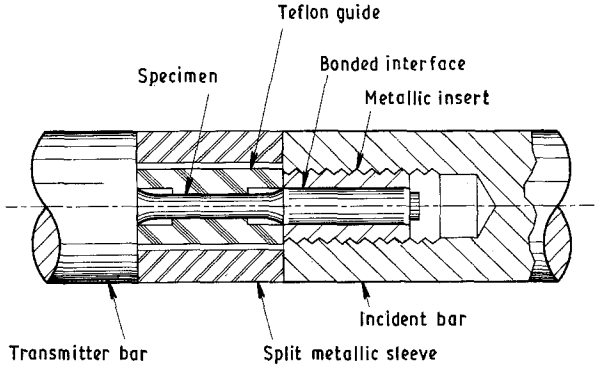

Figure 3 Schematic of SHPB tensile specimen.

3.2. Damage characterization

Failed specimens were examined by optical microscopy, specifically to provide a measure of the spacing of any matrix microcracks. In addition, fracture surfaces were coated with gold, and examined by scanning electron microscopy (SEM).

4. Results

Deformation behaviour is summarized in Fig. 4. Almost hidden in the initial rise of the high strain rate

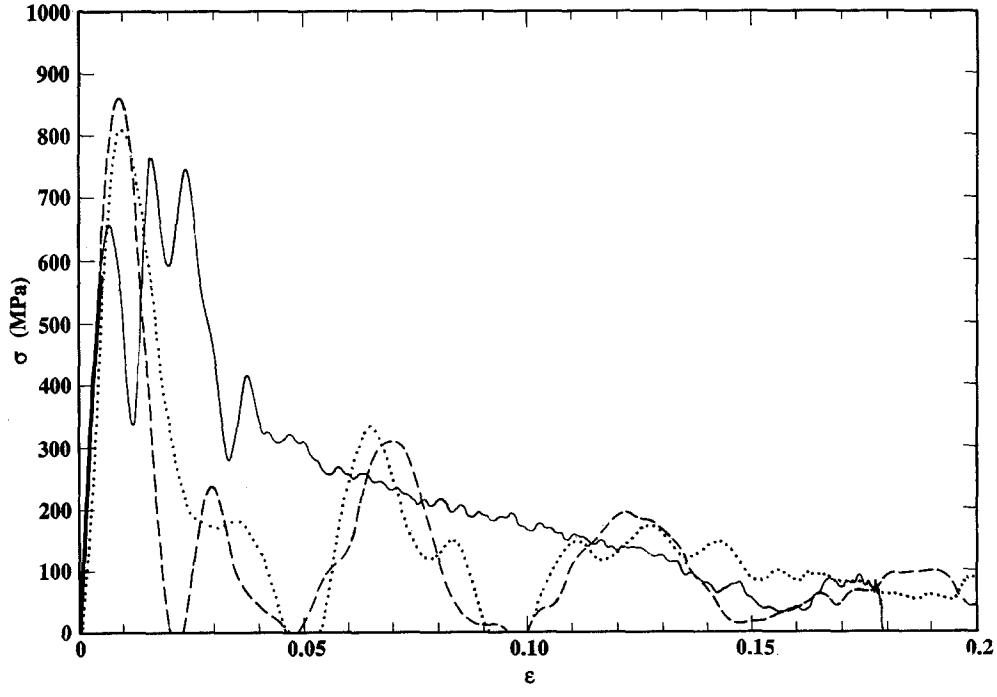

Figure 4 Quasi-static against dynamic stress-strain response (——) 1.15×10^{-5}; (——) 346; (---) 947; (.....) 1100 s^{-1}.

curves lies the complete *quasi*-static stress–strain response; in all the SHPB experiments, the ultimate strength is significantly higher than the *quasi*-static value. At the two highest strain rates, however, the strain at failure (defined as the point of maximum stress) is drastically reduced versus that which obtains at $\dot{\varepsilon} = 346\ s^{-1}$, and there is no obvious yield point. Failure at the latter rate is followed by an extensive regime of continuously declining strength, while in the higher rate dynamic experiments, the post-failure region consists of a series of minor stress–strain peaks of declining amplitude.

Considering the stress–strain curves (Fig. 5) of the two specimens which were characterized by a yield point, σ_0, associated with microcrack initiation, it is evident that σ_0 for both $\dot{\varepsilon} = 1.15 \times 10^{-5}\ s^{-1}$ and $346\ s^{-1}$ is roughly the same, although it is not as accurately defined for the higher rate test. As is generally done in such cases [11], a best fit curve has been drawn through the Pochhammer–Chree oscillations which are typical of the early portions of SHPB stress–strain curves. It should be noted that, while it is possible to achieve a permanent strain of only about 0.001 at a strain rate of $1.15 \times 10^{-5}\ s^{-1}$, a plastic strain of nearly 0.03 is attained when $\dot{\varepsilon} = 346\ s^{-1}$.

Optical examination revealed within the failed specimens periodic matrix microcrack ensembles previously identified [5] as characteristic of non-catastrophic composite failure. Crack spacing data is summarized in Table I, where D, the saturation crack spacing, reflects a count of every crack visible in each specimen. It should be noted that multiple microcracks could not be discerned for the specimens tested at the two highest dynamic strain rates, for which D must then be equal to or greater than the specimen gauge length.

Fibre pull-out was strikingly strain rate dependent, as shown in Fig. 6. Under *quasi*-static conditions (a), the pull-out length varied a great deal. As the loading transits to the dynamic regime (b), this variation is reduced, and so is the average pull-out length; further reduction in pull-out is observed at a still higher strain rate (c). Finally, at the highest strain rate (d), a major change in behaviour occurs, i.e. a large number of fibres are pulled out intact, as evinced by the horizontal coincidence of their originally ground (parallel) ends. It should be noted that this last observation is the physical basis for computing the strain rate attributed to this experiment. Initially, it appeared that the specimen, which on the basis of striker velocity should have endured the highest rate of strain, had not. That is, it did not, when the strain rate was computed in terms of $\dot{\sigma}/E$, which yielded $\dot{\varepsilon} = 897\ s^{-1}$, versus a rate of $947\ s^{-1}$ obtained at the next lowest

TABLE I Crack spacing measurements

$\dot{\varepsilon}$ (s^{-1})	D (μm)
1.15×10^{-5}	310 ± 32
346	515 ± 43
947	⩾ 4445
1100	⩾ 4445

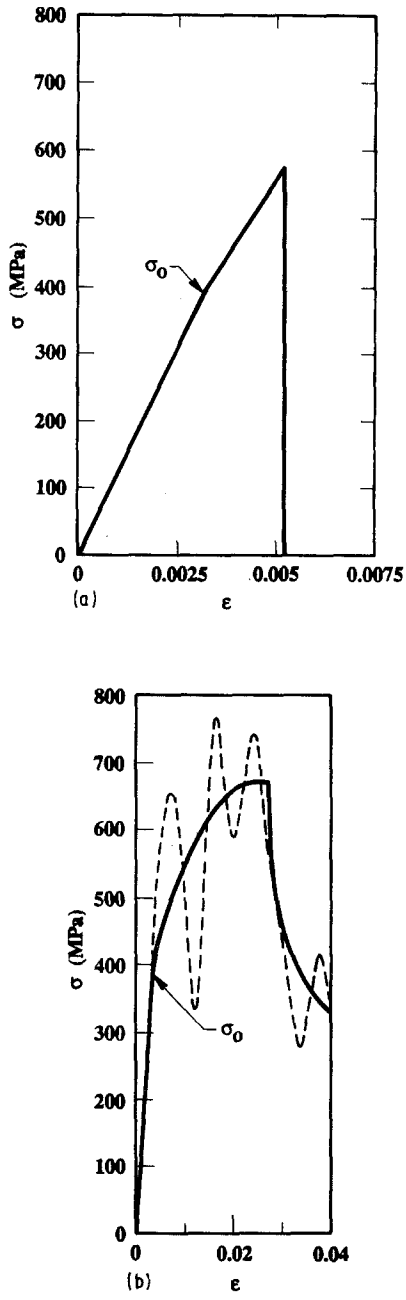

Figure 5 Stress-strain details (a) $\dot{\varepsilon} = 1.15 \times 10^{-5}\ s^{-1}$, showing inelastic yielding; (b) $\dot{\varepsilon} = 346\ s^{-1}$, showing extensive non-linear flow prior to failure.

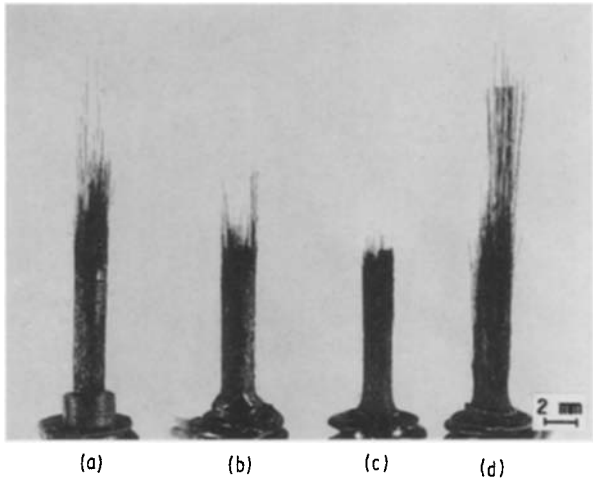

Figure 6 Macroscopic view of specimen failure showing varying degrees of fibre pull out: $\dot{\varepsilon}$ = (a) $1.15 \times 10^{-5}\ s^{-1}$, (b), $346\ s^{-1}$, (c) $947\ s^{-1}$, h (d) $1100\ s^{-1}$.

striker velocity. However, since failure of this anomalous specimen was accompanied by extensive unbroken fibre pull-out, the fibres clearly did not experience the strain, hence did not contribute the stiffness factor, which they would have otherwise. Thus, the effective modulus of the composite must have been lower than E. Assuming a modulus decrease of 15–20%, the actual strain rate, in this case, would be on the order of 1100 s^{-1}. The latter estimate will be used subsequently in correlating results.

In addition to these macroscopic features, the effect of strain rate on fracture mode is manifest at the microscopic level as well. This is demonstrated in dramatic fashion in Fig. 7, where Fig. 7b and d are typical of the appearance of all the SHPB specimens. At slow rates (Fig. 7a), fibres pull out cleanly, and at high magnification (c), the fracture surface has a simple cleavage appearance. On the other hand, under dynamic loading (Fig. 7b), fibres are pulled out attended by globular debris; close inspection (Fig. 7d) indicates that the latter appears to have solidified from a liquid state. The uppermost particle, in fact, is barely attached by a neck apparently solidified just prior to droplet separation.

5. Discussion

It is apparent that under *quasi*-static conditions, the composite behaves in the standard way. The observed stress–strain curve (Fig. 5a) is similar to that reported [9] for identical material tested in a different tensile configuration, and the matrix microcrack spacings (310 μm) are in excellent agreement with those (290 μm) reported [5] for a similar, but not identical Nicalon-LAS system. Based on the wide distribution in fibre pull-out length (Fig. 6a), it is reasonable to assume that the equilibrium nature of the test provided ample opportunity for the stress distribution within the microcracked matrix to sample the statistical flaw distribution within the fibre bundle.

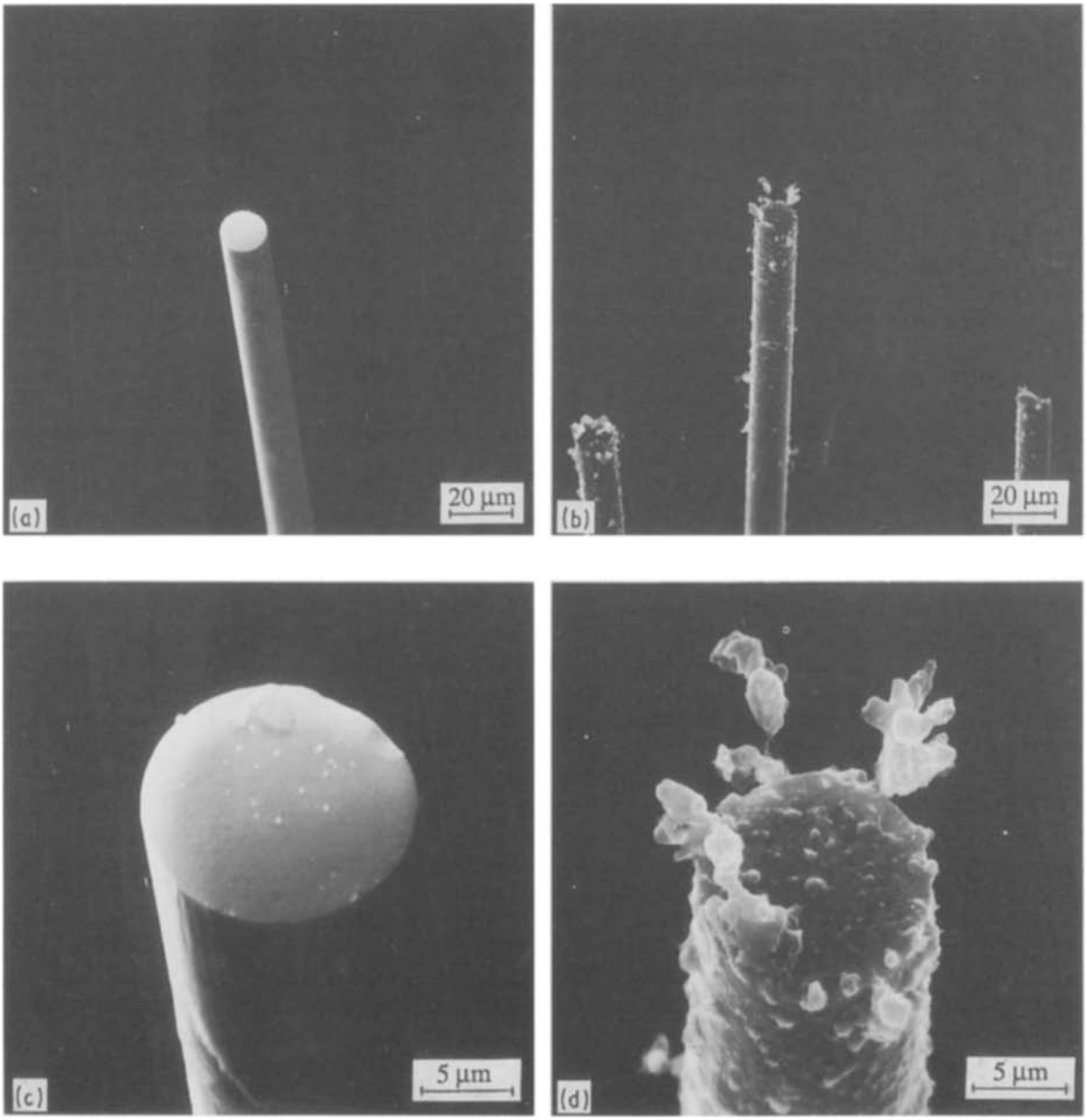

Figure 7 SEM of pulled out fibres: (a) $\dot{\varepsilon} = 1.15 \times 10^{-5}\ s^{-1}$; clean fibres; (b) $\dot{\varepsilon} = 947\ s^{-1}$; debris adhering to fibres; (c) detail of (a); (d) detail of (b).

However, the crack spacing is significantly greater (515 μm) at the lowest dynamic loading rate, and apparently is equal to the specimen gauge length (at least) for still higher rates. The significance of an increasing crack spacing can be explored as follows. First, it has been shown [5] that the sliding shear stress τ and D are related by

$$\tau = \lambda[(1 - f)^2\Gamma_m E_f E_m R^2/fED^3]^{1/2} \quad (1)$$

where λ is equal to 1.34, f is the fibre volume fraction, Γ_m is the matrix fracture energy, R is the fibre radius, and E_f, E_m, and E are the elastic moduli of the fibre, the matrix, and the composite, respectively. Similarly, the threshold stress for matrix cracking can be expressed in terms of a lower bound, steady-state value as

$$\sigma_O = \left[\frac{6\tau f^2\Gamma_m E_f E^2}{(1 - f)E_m^2 R}\right]^{1/3} - \frac{qE}{E_m} \quad (2)$$

where q is the axial residual stress in the matrix. A lower bound estimate for the maximum stress, based on the statistics of simple fibre bundle failure (failed fibres being assumed to have no load bearing capacity, which is not true), is given by [5]

$$\sigma_U = f\hat{S}\exp\left[-\frac{[1 - (1 - \tau D/R\hat{S})^{m+1}]}{(m + 1)[1 - (1 - \tau D/R\hat{S})^m]}\right] \quad (3)$$

with

$$(R\hat{S}/\tau D)^{m+1} = \frac{(A_O/2\pi RL)(RS_O/\tau D)^m}{[1 - (1 - \tau D/R\hat{S})^m]} \quad (4)$$

where $\hat{S}$ is a strength parameter, S_O the Weibull stress scale parameter, m the Weibull modulus, A_O a scale parameter (usually set equal to 1 m^2) and L is the specimen gauge length. In order to use Equation 3, it is necessary to determine $\hat{S}$ by solving Equation 4 numerically, using experimental values for S_O and m. In the present case, $f = 0.46$, $\Gamma_m \cong 20\ Jm^{-2}$ [12], $R = 8$ μm, $E_f = 189$ GPa, $E_m = 85$ GPa, $E = 124$ GPa, $q \cong -50$ MPa [13] (negative q are compressive), and $L = 8.9$ mm. The value of S_O was computed on the basis of [4]

$$A_K S_O^m = 2\pi RLS_1^m/(\ln 2) \quad (5)$$

where S_1 is the median in a Weibull fibre strength distribution. Based on Weibull data generated in tensile experiments performed by Prewo [9] using fibres extracted from the ceramed LAS II matrix, m was found to equal 3.1, and S_O was estimated to be 14.2 MPa.

Based on Equation 3 and the appropriate physical parameters, it is possible to compute the relationship between τ and D shown in Fig. 8. It will be recalled that for two cases, it was possible to measure D, i.e., for $\dot{\varepsilon} = 1.15 \times 10^{-5}\ s^{-1}$, $D \approx 310$ μm, and for $\dot{\varepsilon} = 346\ s^{-1}$, $D \approx 515$ μm, which corresponds to $\tau = 2.2$ and 1.02 MPa, respectively (Table I). In addition, it is clear that for large D values, τ must approach a very low level. Thus, assuming that D for the two highest strain rates were equal to at least half the specimen gauge length, the corresponding value for τ would not exceed 0.038 MPa. These estimates of sliding shear resistance are summarized in Table II.

Also included in Table II are theoretical (Th) and experimental (Exp) values of σ_O (Equation 2) and σ_U (Equation 3). For the two cases in which periodic cracking was observed, the predicted and measured values of σ_O and σ_U are in reasonable agreement; σ_U^{Th} is expected to be a lower bound, in any case. However, the trend in σ_U with decreasing τ is predicted to be slowly decreasing, while it clearly is rapidly increasing (followed by a mild drop when $\dot{\varepsilon} = 1100\ s^{-1}$).

It is obvious that the theoretical model [5] is inconsistent with the physical events attending failure at higher strain rates. In particular, following the nucleation of the dominant matrix crack, fibres begin to slide at such a rate that τ drops precipitously. Until that time, τ must be of the order 1–2 MPa, and the dominant cracks probably form at a stress level much higher than the predicted 138 MPa.

Values of τ as low as 0.038 MPa, combined with the observation of globular debris associated with fibre pull-out, suggest that the matrix is melting during fibre sliding. This is not as unreasonable as it might seem, given the apparent velocities involved in the pull-out process. For the highest strain rate, $1100\ s^{-1}$, fibres are extracted over a distance of approximately 4.5 mm in about 2 μs. This corresponds to a sliding speed of $2250\ m\,s^{-1}$, a rate which would probably

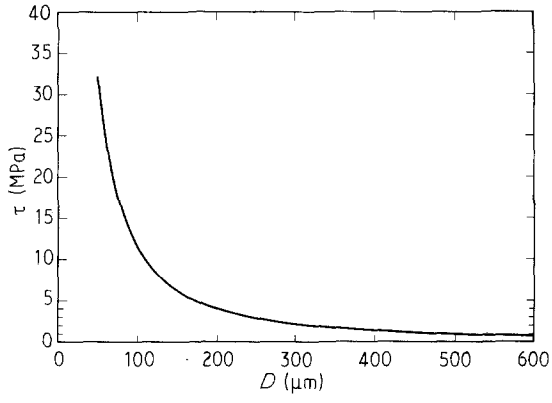

Figure 8 Debonded interfacial shear resistance against matrix crack spacing.

TABLE II Theoretical and experimental fracture parameters

$\dot{\varepsilon}$ (s^{-1})	τ (MPa)	σ_O^{Th} (MPa)	σ_O^{Exp} (MPa)	σ_U^{Th} (MPa)	σ_U^{Exp} (MPa)
1.15×10^{-5}	2.2	303	395	433	585
346	1.02	253	380	429	683
947	0.038	138	–	420	868
1100	0.038	138	–	420	810

produce immense frictional heating, even in so short a time.

It is interesting to consider the strength–strain rate dependence for the three dynamic experiments. Once the strain rate exceeds some critical value, situated between 346 and 947 s^{-1}, the specimen contains only one major crack, the faces of which are bridged by fibres sliding with little resistance within the matrix. Because τ is so low, frictional load transfer is insufficient to load the sliding fibres to the level necessary to sample their Weibull flaw distribution. Only those fibre segments bridging, and extending a short distance below, the main crack interface experience high stresses, and these segments are short—so short that the fibres must fail at sites other than their weakest links.

Thus at $\dot{\varepsilon} = 947\ s^{-1}$, fibres are sliding throughout the specimen when the stress level near the interface reaches a level sufficient to break a number of the fibres. The over-all stress level drops, as the load is transferred to the remaining stronger fibres, causing the load to increase again (the first post-failure peak in Fig. 4), a process which is repeated several times until all the fibres have failed in the near-interface region of the main crack. On the other hand, at $\dot{\varepsilon} = 1100\ s^{-1}$, the sliding shear resistance is sufficiently low that just below the stress level required to fail the most highly stressed fibres, they break free all along the specimen length, creating the first load drop (failure), following which subsequent load transfer and near-interface fibre fracture proceed as described above.

The crucial implication of this scenario is that at even higher strain rates, the ultimate strength may be even further reduced, in which case the strength eventually would approach that required simply to create the first matrix crack. Experiments at higher rates of loading clearly are required in order to test the validity of this hypothesis.

Acknowledgements

The authors are grateful for the support of the Office of Naval Research under Contract N00014–83–C–0213.

References

1. R. W. GOETTLER and K. T. FABER, *Comp. Sci. Tech.* **37** (1989) 129.
2. D. C. PHILLIPS, *J. Mater. Sci.* **9** (1974) 1847.
3. A. G. EVANS and D. B. MARSHALL, *Acta Metall.* **37** (1989) 2567.
4. M. D. THOULESS, O. SBAIZERO, L. S. SIGL and A. G. EVANS, *J. Amer. Ceram. Soc.* **72** (1989) 525.
5. H. C. CAO, E. BISCHOFF, O. SBAIZERO, M. RUHLE and A. G. EVANS, *ibid.* **73** (1990) 1691.
6. D. B. MARSHALL and W. C. OLIVER, *ibid.* **70** (1987) 542.
7. D. C. CRANMER, *Com. Amer. Ceram. Soc.* **67** (1984) C180.
8. D. B. MARSHALL, in "Ceramic Microstructures: The Role of Interfaces", edited by J. A. Pask and A. G. Evans (Plenum Press, New York, 1988) p. 859.
9. K. M. PREWO, in "Advanced Characterization of SiC Fiber Reinforced Glass-Ceramic Matrix Composites" (ONR Interim Report, Contract No. N00014-81-C-0571; June 1983).
10. J. J. BRENNAN, in "Additional Studies of SiC Fiber Reinforced Glass-Ceramic Matrix Composites" (ONR Annual Report, Contract No. N00014-82-C-0096, April 1984).
11. T. NICHOLAS, *Exp. Mech.* **21** (1981) 177.
12. T. J. CLARK and J. S. REED, *Amer. Ceram. Soc. Bull.* **65** (1986) 1506.
13. D. B. MARSHALL and A. G. EVANS, *J. Amer. Ceram. Soc.* **68** (1985) 225.

Received 10 April
and accepted 1 May 1991